Journal of Materials Chemistry A

Accepted Manuscript

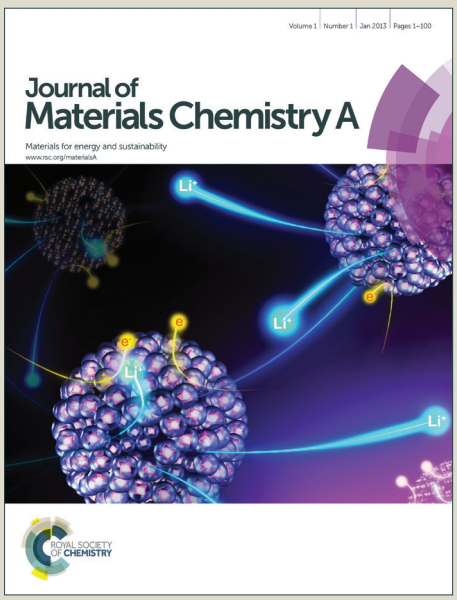

ROYAL SOCIETY OF CHEMISTRY

www.rsc.org/materialsA

NMR study of Li distribution in $Li_{7-x}H_xLa_3Zr_2O_{12}$ garnets.

G. Larraz[1], A. Orera*[1], J. Sanz[2], I. Sobrados[2], V. Diez-Gómez[2], M. L. Sanjuán[1]
[1]Instituto de Ciencia de Materiales de Aragón, CSIC - Universidad de Zaragoza,
E- 50009 Zaragoza, Spain
[2]Instituto de Ciencia de Materiales de Madrid, CSIC,
E-28049 Madrid, Spain

Abstract

Despite the large number of NMR studies performed on lithium conductors with the garnet-type structure, the distribution of the lithium ions in $Li_7La_3Zr_2O_{12}$ (LLZO) and their contribution to ionic conductivity are still a matter of controversy.

In this work we present a magic-angle spinning (MAS) NMR study of enriched $^6Li_{7-x}H_xLa_3Zr_2O_{12}$ ($0 \leq x \leq 5$) garnets with the aim of identifying the bands arising from the different lithium sites occupied in the garnet lattice. Taking advantage of the known sensitivity of this material to moisture and facile proton-for-lithium exchange, we have been able to alter the relative population of tetrahedral and octahedral sites (the exchange is favoured in the latter) by submitting the samples to different post-treatments so as to obtain samples with varying lithium content. This has allowed the identification of three different bands that we ascribe to Li in different environments within the garnet structure. Besides, variable temperature measurements have put into evidence the presence of dynamic exchange processes between octahedral and tetrahedral Li sites.

Protons inserted in the garnet structure have also been analyzed by means of ^{1}H-MAS-NMR and Raman spectroscopies. ^{6}Li-^{1}H-CP-MAS experiments have allowed the investigation of the relative distribution of protons and lithium ions in partially exchanged samples.

Introduction

The family of $Li_{3+y}La_3M_2O_{12}$ lithium-conducting garnets (M= Nb, Ta, Sb, Zr,…) has attracted interest in the last ten years as candidates to be used as electrolytes in lithium batteries (see review by Thangadurai et al. and references therein).[1] Among them, those with tetravalent M cation are particularly interesting since their stable structure is tetragonal ($I4_1/acd$ Space Group (S.G.)), in contrast with the cubic symmetry ($Ia\bar{3}d$) of garnets with pentavalent or hexavalent M cation. Despite their low conductivity (1.63×10^{-6} S/cm for tetragonal $Li_7La_3Zr_2O_{12}$ (t-LLZO) and $\sim 10^{-8}$ S/cm for $Li_7La_3Sn_2O_{12}$, both at 300 K)[2,3] tetragonal garnets serve as model materials to understand the role of site occupancies.

The low conductivity of the tetragonal garnets was soon attributed to the fully ordered distribution of lithium in three crystallographic sites of the $I4_1/acd$ unit cell: the 8*a* site, with nearly regular tetrahedral symmetry, and two distorted octahedral sites 16*f* and 32*g*, where lithium is either slightly displaced from the octahedron center in the first one, or clearly shifted toward an octahedron face in the second.[2,3] Thus, in the tetragonal garnets two thirds of the tetrahedral cavities of the prototype garnet structure are empty whereas all the octahedral sites are occupied. In parallel, the high conductivity of cubic garnets arises from the partial occupancy of both tetrahedral (24*d*) and octahedral (48*g* and 96*h*) cages. For the lowest lithium contents the higher occupancy of the tetrahedral site results in the shift of all neighbouring octahedral lithium ions to the more distorted site (96*h* in $Ia\bar{3}d$ S.G.).

As regards Zr-based garnets, since the first report by Murugan et al.[4] of a highly conducting cubic form of $Li_7La_3Zr_2O_{12}$ (c-LLZO) (later explained as a result of accidental Al-doping from crucibles)[5] current efforts are now devoted to optimize its conductivity by appropriate doping either at the Li or Zr sublattices [6-13] , and even by varying the rare earth.[14] In parallel, intense theoretical work is being carried on to model the lithium conduction paths and the role of octahedral and tetrahedral sites in the diffusion mechanism. [15, 16, 17]

Altogether, it is clear that a delicate interplay exists between lithium content, site occupancy and total conductivity, which puts into evidence the need of a thorough characterization of the lithium distribution in tetragonal and cubic LLZO phases, as well as of its evolution with temperature.

In the context of lithium conducting oxides, solid-state NMR spectroscopy is a highly valuable technique that provides information about structural and dynamic aspects. [18, 19] Structural information is mainly obtained from high resolution [6,7]Li-MAS-NMR when this is able to identify bands arising from the different lithium species present in the lattice. Through appropriate modeling, a relation between chemical shifts and Li environment can be proposed. [20, 21, 22] Since the NMR intensity is proportional to the lithium concentration, a comparison of the integrated areas provides a hint of the lithium occupancy of each site. Information on lithium diffusion, on the other hand, is obtained either from lineshape analysis of static NMR spectra as a function of temperature or from relaxometry experiments.[23]

The situation in Li-conducting garnets is however complicated by several factors: first, the range of Li chemical shifts (δ_{iso}) in these materials is very narrow, which makes it difficult to perform an unambiguous assignment to specific lithium sites. This is especially critical when only ^{7}Li spectra are recorded, since dipolar broadening, even in MAS spectroscopy, obscures the eventual separation of bands with different δ_{iso}. ^{6}Li MAS-NMR provides a much higher resolution, but has the disadvantage of a lower signal to noise sensitivity since this isotope is only 7% abundant in natural lithium. To these intrinsic difficulties another one has to be added, namely the presence of lithium-containing impurities. This aspect is often underestimated, an omission that is particularly relevant in Li garnets due to the tendency of these compounds to form second phases such as lithium hydroxides or lithium carbonate as a result of the facile exchange of lithium by protons from ambient air.[24, 25, 26] A simple explanation for this contribution being frequently disregarded is that most of such phases are light-weight compared with the garnet itself, which makes them not easily detectable by X-ray diffraction routinely used to characterize the phase purity of the samples.

Concerning ^{6}Li-MAS-NMR measurements in the LLZO-based garnets, for instance, Kuhn et al [27] find two bands at around 0 and +1.2 ppm that were initially attributed to tetrahedral and octahedral sites, respectively, though in a subsequent publication they suggest that the signal at lower δ_{iso} values, may arise from Li_2CO_3.[28] In contrast, Geiger et al. find a single band around 1.2-1.3 ppm in cubic, Al-stabilized c-LLZO.[5] The chemical shift values and the narrow linewidths lead these authors to attribute this band to the tetrahedral sites, where lithium would spend most of their time. As regards ^{6}Li-MAS spectra of related garnet compounds, Van Wüllen et al. find two bands for $Li_5La_3Nb_2O_{12}$ at slightly different chemical shifts but separated by the same interval of about +1.2 ppm, that they attribute to tetrahedral and octahedral species (at lower and higher δ_{iso} values, respectively).[29] Two bands are also found in $Li_5La_3Nb_2O_{12}$ and $Li_5La_3Ta_2O_{12}$ by Nyman et al. and interpreted as arising from “non-mobile” and “mobile” lithium ions of the garnet lattice.[30] A very similar result is reported by Spencer et al. for $Li_6BaLa_2Ta_2O_{12}$ and $Li_6BaLa_2Nb_2O_{12}$.[31] Finally, for the other tetragonal garnet $Li_7La_3Sn_2O_{12}$, with a Li distribution similar to LLZO, Galven et al. find just one peak at +1.7 ppm in the ^{6}Li-MAS spectrum of the stoichiometric compound and two signals, at +1.7 and +1 ppm, in the proton-exchanged variety.[24] Due to the higher broadening effects, as explained above, a single band has been systematically found in ^{7}Li-MAS spectra [5, 32, 33, 34, 35]. Diffusion parameters have also been determined by a number of authors, either through lineshape analysis of ^{7}Li spectra as a function of temperature or by relaxometry. [7, 27, 31, 36, 37,, 38]

In this work we present an NMR study of LLZO garnets with the aim of identifying the bands arising from the different lithium sites occupied in the lattice. To gain both resolution and sensitivity we present (for the first time to our knowledge) ^{6}Li-MAS-NMR spectra recorded in samples enriched with the ^{6}Li isotope. Taking benefit of the known sensitivity of this material to moisture and facile proton-for-lithium exchange, we have been able to alter the relative population of tetrahedral and octahedral sites by submitting the samples to different post-treatments so as to obtain samples with varying lithium content. The characteristics of proton bonding have also been analyzed by means of ^{1}H-MAS-NMR, ^{6}Li-^{1}H -CP-MAS-NMR and Raman spectroscopies. Variable temperature measurements have put into evidence the presence of dynamic processes.

Experimental

Sample preparation:

Powdered samples of tetragonal $Li_7La_3Zr_2O_{12}$ garnet have been synthesized by solid state reaction at temperatures between 900 °C and 980 °C using $^6LiOH{\cdot}H_2O$ (95 atom % ^6Li) or $^7Li_2CO_3$ (99% purity), La_2O_3 (99.99% purity, pre-dried at 900 °C for 12 h) and ZrO_2 (99% purity) as reagents. 15% excess of lithium was added to the stoichiometric ratio to compensate lithium loss during the synthesis.

In order to vary the lithium content in the garnet, Li^+/H^+ exchange was performed by submitting a fresh tetragonal sample to prolonged annealing in air both at 350 °C and at RT. In addition to the garnet phase, lithium hydroxide and lithium carbonate were detected as secondary phases coming from the proton for lithium exchange process. Both phases are water soluble, so, with the aim of clarifying the NMR spectra, the aged samples were dipped in water for 2 min under stirring and then filtered and dried. By means of XRD and Raman Spectroscopy we have verified that no changes take place in the garnet after the washing treatment so that only the secondary phases were removed.

Sample Characterization:

The chemical composition of the synthesized materials was determined by ICP-OES (inductively coupled plasma optical emission spectrometry). Within the experimental error, the La and Zr content were close to the stoichiometric composition.

X-ray diffraction (XRD) experiments were performed on a Rigaku D/max 2500 diffractometer equipped with Cu Kα (λ = 1.5418 Å) radiation and working at 40 kV and 80 mA. Data were collected in a step mode with Δ2Θ = 0.03° and a counting time of 1 s per step. XRPD patterns were analyzed by the Rietveld method[39] using the FullProf software.[40]

Raman dispersion measurements were performed using a DILOR XY spectrometer with a CCD detector and a spectral resolution of 1.4 cm^{-1}. The 514.53 nm line of an Ar^+ ion laser was used as the excitation source, the power at the sample surface being ≤25 mW. The scattered light was collected through an X50 microscope objective lens. A Linkam TS1500V stage was used for *in situ* thermal treatments.

Thermogravimetric analysis (TGA) was carried out in a SDT2960 thermobalance, with a heating rate of 10 °C min^{-1} in the temperature range from 25 to 650 °C under flowing air.

Single pulse ^1H, ^7Li and ^6Li MAS and $^6Li\{1H\}$ -CP-MAS NMR experiments were conducted on a Bruker Avance-400 NMR spectrometer with a 9.4 T widebore superconducting magnet. The measurements were performed with 2.5 mm zirconia rotors with Kel-F caps and a spinning rate of 10 and 20 kHz. In high-power proton decoupling experiments ^6Li nuclei were irradiated with a π /2 pulse, the relaxation delay used was 80s, 32 scans were acquired and a proton decoupling SPINAL64 sequence was used.

^1H MAS NMR spectra were recorded at 400.13 MHz after excitation with a π/2 pulse length of 3.2 μs and a recycle delay of 90s. The number of scans was 8. Spectra were referenced to TMS (Tetramethylsilane). The single pulse ^6Li MAS NMR spectra were studied at 58.86 MHz after irradiating the samples with a π/8 (1 μs) pulse, a relaxation delay of 40 s and 80 scans. ^7Li MAS NMR spectra were obtained at 155.51 MHz, after π/2 (1.75μs) pulse irradiation, a relaxation delay of 10 s and 120 scans. Chemical shifts refer to an aqueous solution of LiCl (1 M). Some experiments have been conducted at higher relaxation delays (15000 s), to avoid saturation effects in the detection of Li signals with long relaxation delays. For comparison purposes, ^6Li MAS NMR spectra were recorded for reference materials of the H^+/Li^+ exchange process by-products, and signals at 0.1, 1.2 and 0.02 ppm were observed for Li_2CO_3, LiOH and $LiOH{\cdot}H_2O$ respectively.

^6Li-^1H-CP-MAS-NMR spectra were recorded in selected samples after a contact time of 7 ms and 64 scans. The relaxation delay was 60s without acquisition of dummy scans. Hartman-Hann polarization transfer from ^1H to ^6Li was achieved with a nutation frequency of 70kHz. During acquisition a proton decoupling SPINAL64 sequence was used.

The nature of the cross-polarization process, in which ^{6}Li spin gathers higher polarization from the proton-spin reservoir, restricts detection of lithium nuclei to those located near protons, namely, only those lithium nuclei which have dipolar interactions with proton nuclei. Spin-lattice relaxation behavior was studied by using the inversion-recovery pulse sequence (180º-τ-90º); the 90º pulse length was 4us, tau was varied from 0 to 100 s, a relaxation delay of 100 s was used , and 8 scans were acquired for each time step.

Experimental Results and Discussion

1. X-ray powder diffraction and chemical analysis

The XRD patterns of natural abundance and ^{6}Li enriched fresh-synthesized $Li_7La_3Zr_2O_{12}$ garnets are shown in Fig. 1, highlighting the good crystallinity and high quality of the samples. Both diffractograms were indexed in the tetragonal $I4_1/acd$ space group, with lattice constants a= 13.1118 (4) Å, c= 12.6571 (4) Å and a=13.106 (1) Å, c=12.661 (1) Å respectively, in agreement with those reported in the literature. [2]

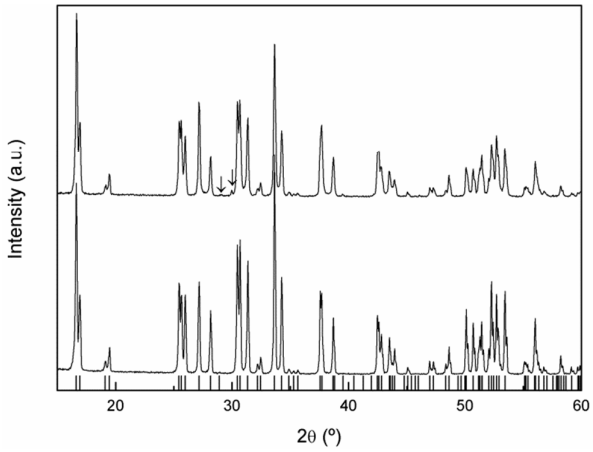

Figure 1. XRD patterns of natural abundance (bottom) and ^{6}Li enriched (top) fresh-synthesized tetragonal $Li_7La_3Zr_2O_{12}$ garnets. Bars denote the reflections allowed for $I4_1/acd$ space group. Peaks denoted with the symbol ↓ correspond to La_2O_3.

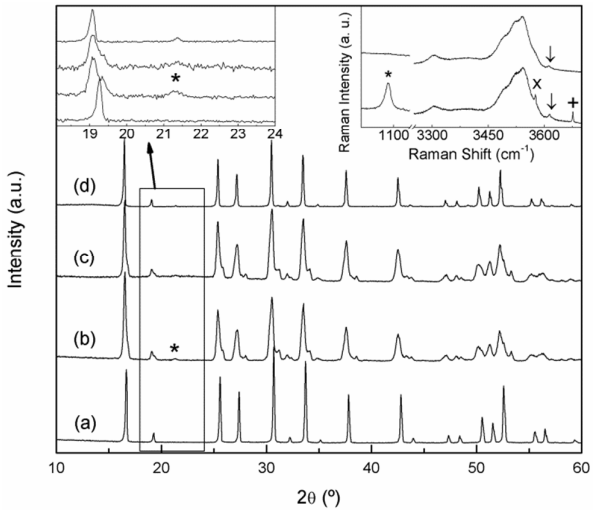

Figure 2. XRD patterns of $Li_7La_3Zr_2O_{12}$ sample a) washed after aging at 350 °C, b) aged at room temperature, c) washed after ageing at room temperature, d) sample in c) after heating at 300 °C. Left inset: XRD zoom. Right Inset: High frequency Raman spectra of the RT aged sample before (bottom) and after (top) washing. Symbols *, x, + and ↓ denote Li_2CO_3, $LiOH{\cdot}H_2O$, LiOH and $La(OH)_3$ respectively.

In a previous work[26] we reported on the sensitivity of $Li_7La_3Zr_2O_{12}$ garnet to ambient conditions, especially to exposure to moisture. Annealing the material in air at temperatures of the order of 300 ºC resulted on a partial H^+/Li^+ exchange and the transformation of the tetragonal phase to a cubic garnet. The XRD pattern of this annealed

sample (Fig. 2a) shows a single phase cubic garnet that was indexed in the $Ia\bar{3}d$ space group with a = 13.0034 (3) Å. The space group of this protonated material is that of the conventional cubic garnets[41] and the high temperature phase of tetragonal $Li_7La_3Zr_2O_{12}$ above 650 °C.[26]

However, an analogous H^+/Li^+ exchange process can take place at room temperature after long storage times. As it is clear from Fig. 2b, that shows the XRD pattern of a $Li_7La_3Zr_2O_{12}$ sample 3 years after the synthesis, the material overcomes the aforementioned phase change to a cubic symmetry, although it is not completely homogeneous and remains of the tetragonal phase can be observed. A subsequent treatment with water (Fig. 2c) washes out the secondary phases that appear as result of the exchange process, identified by means of Raman spectroscopy as Li_2CO_3, LiOH and $LiOH{\cdot}H_2O$ (inset at the right of Fig. 2). As lithium has a low X-ray scattering factor, Raman spectroscopy is extremely useful to identify Li-containing secondary phases. The spectra in the 1000 cm^{-1} region highlight the possible presence of Li_2CO_3, unambiguously identified by its band at ~ 1090 cm^{-1}. On the other hand, hydroxide secondary phases are easily identified by their OH^- stretching vibrations, typically appearing between 3500 and 3700 cm^{-1}. The spectra in this region show, together with the characteristic bands associated to LiOH and $LiOH{\cdot}H_2O$ (3675 and 3575 cm^{-1}, respectively) different broad bands corresponding to protons in the exchanged garnet. These Raman features will be explained in a later section.

When this washed sample is briefly heated at 300°C its homogeneity increases and a single phase cubic garnet is obtained (Fig.2d), although some weak reflections can not be explained with the $Ia\bar{3}d$ space group. While higher resolution diffraction techniques would be required to study the structure of this exchanged compound, a first approximation could be proposed following Galven et al.'s work on the related $Li_{6-x}H_xCaLa_2Nb_2O_{12}$ garnet,[42] that is indexed with the non-centrosymmetric space group $I\bar{4}3d$ taking into account second harmonic generation, transmission electron microscopy and powder neutron diffraction data. In our case, changing from $Ia\bar{3}d$ to $I\bar{4}3d$ would index the low intensity peaks observed at 21.5, 40.3 and 53.4 °.

The stoichiometry of the exchanged materials was determined by ICP analysis of the washed samples (without second phases) and supported by the results obtained from TGA experiments, leading to a composition of $Li_{4.8}H_{2.2}La_3Zr_2O_{12}$ for the sample annealed at 350°C and $Li_{3.8}H_{3.2}La_3Zr_2O_{12}$ for the sample aged at room temperature (H^+ content calculated for electrical neutrality). The lower symmetry of the compound aged at RT, compared to that exchanged at 350 °C, is then tentatively ascribed to its higher proton content together with the difference in the temperature at which exchange is performed.

It is worth noting that similar or even higher exchange states can be reached by treatment in water at reflux for several days. In this case, the absence of CO_2 in the exchange media hinders the carbonation of LiOH exchange product to Li_2CO_3. A detailed comparative study of the different exchange states will be published elsewhere.

2. Li-MAS-NMR of $Li_7La_3Zr_2O_{12}$ and $Li_{7-x}H_xLa_3Zr_2O_{12}$

Both the ^{7}Li-MAS-NMR and ^{6}Li-MAS-NMR spectra recorded for the sample synthesized using natural abundance Li_2CO_3 are compiled in Fig. 3. The former spectrum exhibits one central broad band at approximately +1.2 ppm and up to three rotational sidebands. The large width of the ^{7}Li-NMR signal confirms the need of ^{6}Li-NMR measurements in order to distinguish Li atoms in different crystalline sites of the garnet structure, as suggested by other authors.[29] In fact, ^{6}Li-MAS-NMR spectra of the same sample shows additional bands besides the main signal centred at +1.2ppm.

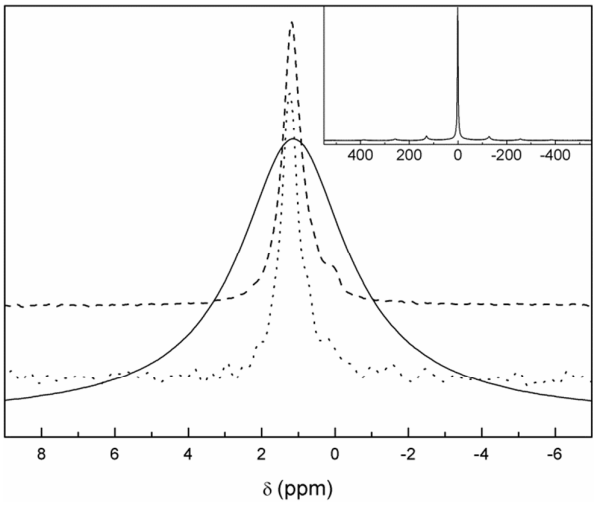

Figure 3. Zoom of the central band of ^{7}Li (solid) and ^{6}Li-MAS-NMR (dotted) spectra of t-LLZO synthesized with natural abundance Li_2CO_3 compared to ^{6}Li-MAS-NMR (dashed) spectrum recorded in $^{6}Li_7La_3Zr_2O_{12}$. Inset: Full ^{7}Li-MAS-NMR spectrum of as-synthesized t-LLZO.

In order to obtain better signal-to-noise ratios, the ^{6}Li-MAS-NMR spectrum has been recorded in the enriched $^{6}Li_7La_3Zr_2O_{12}$ sample (Fig.3) for the first time to our knowledge. At least two NMR bands can be clearly distinguished in this spectrum: the main +1.2 ppm band and a less intense one at ~+0.1 ppm. Kuhn et al. already reported two signals centred at identical chemical shifts, and attributed the low chemical shift band very likely to Li_2CO_3.[28] Our NMR experiments on tetragonal $Li_7La_3Zr_2O_{12}$ samples with different ageing and annealing conditions confirm this attribution, since the intensity of the signal close to +0.1 ppm varies significantly and in agreement with the amount of Li_2CO_3 observed in the Raman spectra. It's interesting to note that long relaxation delays were needed to avoid saturation of the +0.1 ppm signal, as proposed by Kuhn in his work. The assignment of the low δ_{iso} band to a secondary phase instead of the tetrahedral Li sites has some important implications concerning the diffusion model, as it will be shown later[29, 36, 37].

Since the total amount of lithium decreases due to the H^+/Li^+ exchange, as reported in the previous section, we have made use of the protonated samples in order to clarify the real nature of the main band at +1.2 ppm and its possible asymmetry.

Fig. 4 shows the ^{6}Li-MAS NMR spectra of $^{6}Li_7La_3Zr_2O_{12}$ as prepared and after ageing at room temperature. As it has been mentioned, the intensity of the +0.1 ppm band clearly increases after ageing, in accordance with the higher amount of lithium carbonate formed in the sample from the proton exchange. In fact, when the sample is washed until no impurities are observed in the Raman spectrum (inset of Fig.2), this NMR band disappears. This washing step also reduces the intensity of the band at ~ +1.2ppm, due to the removal of the lithium hydroxide produced with the proton exchange process. Therefore, from the combination of XRD and Raman data we can conclude that all the ^{6}Li signals detected in the washed aged sample ($Li_{3.8}H_{3.2}La_3Zr_2O_{12}$) are characteristic of the garnet and correspond to different Li environments in the cubic structure.

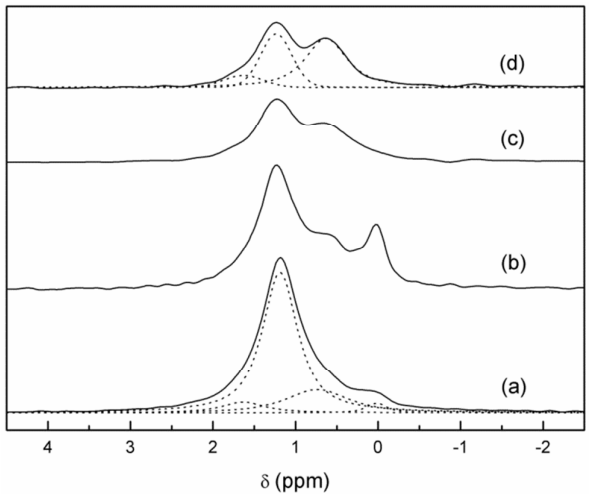

Figure 4. ^{6}Li-MAS-NMR spectrum of $^{6}Li_7La_3Zr_2O_{12}$ as prepared (a) and aged at room temperature, $^{6}Li_{3.8}H_{3.2}La_3Zr_2O_{12}$, before (b) and after the washing step without (c) and with (d) ^{1}H decoupling. The four spectra are normalized to the total Li content, as determined by ICP. Dotted lines show the components result of the fitting

The ^{1}H-decoupled spectrum of $Li_{3.8}H_{3.2}La_3Zr_2O_{12}$ has been decomposed as a sum of bands with pseudo-Voigt profile. This yields three components: two clearly distinguishable bands at +0.6 and +1.2 ppm and a third one at approximately +1.6 ppm only seen as a shoulder of the main band (Fig. 4). A determination of the relative intensities of these three bands is difficult because of the considerable overlapping between them. The relative areas of these lines depend also on the Gaussian or Lorentzian character of each component, which can be largely varied without appreciable loss of fit quality. The results of representative fitting approaches are included in Table 1.

Sample	δ ^{6}Li (ppm)	%	Li per garnet mol
$Li_{3.8}H_{3.2}La_3Zr_2O_{12}$	1.6	10	0.37 ± 0.15
	1.2	35	1.33 ± 0.15
	0.6	55	2.1 ± 0.1
$Li_7La_3Zr_2O_{12}$	1.6	7	0.50 ± 0.20
	1.2	70	4.8 ± 0.8
	0.7	20	1.5 ± 0.5
	0.1	3	0.2 ± 0.05

Table 1. Fitting results of the ^{6}Li-MAS-NMR spectrum of $^{6}Li_{3.8}H_{3.2}La_3Zr_2O_{12}$ (^{1}H decoupling) and as prepared $^{6}Li_7La_3Zr_2O_{12}$

Considering that the available sites for lithium in the crystal are basically the same in both compounds, an extrapolation of the bands resolved in $Li_{3.8}H_{3.2}La_3Zr_2O_{12}$ can be made to the $Li_7La_3Zr_2O_{12}$ spectrum. From the fit shown in Fig.4 it is clear that the asymmetric central band of the $Li_7La_3Zr_2O_{12}$ spectrum can be fitted with the three components in +0.6, +1.2 ppm and +1.6 ppm. The difficulty in calculating the proportion of each lithium site, together with the lack of a reliable model for the relationship between the chemical shift and the chemical coordination of the atom, makes the assignment of the three bands to different crystal sites complicated. However, comparing both spectra and having in mind the process that has taken part between both states of the garnet we can propose an attribution for these bands.

First of all, based on the high intensity of the +1.2 ppm band in the as-grown (AG) sample and taking into account the site occupancy in t-LLZO,[41] we assign that band to the more distorted octahedral Li ions (oct2). This assignment is supported by physical arguments related to the exchange process: since model calculations predict a lower activation for this site,[16] it is reasonable to assume that these Li ions are more easily exchanged than tetrahedral ones. Then, the significant decrease of the +1.2 ppm band in the protonated garnet, compared to the AG one, can be straightforwardly attributed to the easier exchange of Li ions from the more distorted octahedral site at RT (see Fig.

SP1 in the supplementary information file for a variation of the intensity of this band as a function of the degree of H^+/Li^+ exchange).

The attribution of the two other lateral bands is not as straightforward. If we compare the spectra of the as-prepared and exchanged samples, the band centred at +0.6 ppm slightly increases after ageing. The tetrahedral sites in the tetragonal parent compound are just partially occupied[2] and provide potential hopping sites in the conduction process,[41] so they could increase their occupancy during the exchange process.[16] In consequence, the H^+/Li^+ exchange would not only affect one specific Li environment, but also favour certain lithium redistribution and the increase of tetrahedral site occupancy. Thus, the band at +0.6 ppm is attributed to tetrahedral lithium ions.[43] The origin of the third band at +1.6 ppm is not clear but could be related to the less distorted octahedral lithium sites (oct1).

With this preliminary assignment, an analysis of the tetragonal parent compound can be made. As explained previously, the signal centred at +0.1 ppm can be directly assigned to the presence of lithium carbonate, probably due to both a low lithium excess from the synthesis and a slight H^+/Li^+ exchange, and accounts for approximately 3% of the total lithium content. Lithium sites in t-LLZO have been described by several authors to consist of 1 tetrahedral site (8*a*) and 6 octahedral sites: 2 weakly distorted (16*f*) and 4 highly distorted (32*g*).[2, 11, 41] In our case, the relative intensities of the three components of the spectrum (Table 1) would correspond to 1.5 lithium ions in the tetrahedral site, 0.5 in the less distorted octahedral site and 4.8 in the highly distorted octahedral site, assuming a total content of 7 lithium ions per formula. This disagreement with the reported theoretical values could arise from the enormous avidity for water of these garnets and the fact that even the as prepared tetragonal sample is slightly exchanged, as will be shown in the following section. This exchange is even more favoured by the powdered state of the sample that highly increases the surface area exposed to moisture.

Measurements of the spin-lattice relaxation times as a function of temperature support the hypothesis of lower activation energies for octahedral sites, the T1 values of oct1 and oct2 sites being shorter than those of tetrahedral sites (see supplementary information). This result also agrees with the finding of dynamic properties reported in section 4.

3. Raman, ^{1}H-MAS-NMR and ^{6}Li-^{1}H-CP-MAS-NMR of $Li_{7-x}H_xLa_3Zr_2O_{12}$

Proton incorporation in the garnet structure after ageing at RT in air has been confirmed by Raman spectroscopy measurements in the OH-region (inset of Fig.2) and TGA (Fig.5). Regarding the former, ageing at RT leads to the appearance of several bands in the 3200-3700 cm^{-1} region, characteristic of the stretching vibrations of hydroxyl entities. In addition to the narrow bands at 3575, 3610 and 3675 cm^{-1}, arising from $LiOH{\cdot}H_2O$, $La(OH)_3$ and LiOH, respectively, an intense band is found extending from 3450 to 3600 cm^{-1}, together with another broad feature around 3300 cm^{-1}. The main band, in turn, can be decomposed in four components, with maxima at 3490, 3521, 3545 and 3570 cm^{-1} (see Fig. SP2 in supplementary information).

The appearance of several components in the high frequency band can be related to the presence of non-equivalent oxygen sites in the lattice or to different configurations of proton bonding. These frequencies are somewhat lower than those of covalently bonded hydroxyl anions, which are typically above 3600 cm^{-1},[44] thus suggesting that some degree of hydrogen bond is present between the hydroxyl proton and another oxygen atom, as in an O-H…O configuration. As the oxygen-oxygen distance ($d_{O\text{-}O}$) shortens the hydrogen bond becomes stronger, resulting in a reduction of the stretching frequency $\nu_{O\text{-}H}$. In fact, a close correlation is empirically found between $\nu_{O\text{-}H}$ and $d_{O\text{-}O}$. Using the expression $\nu_{O\text{-}H} = 3592\text{-}304\text{x}10^9.\exp(-d_{O\text{-}O}/0.1321)$ given by Libowitzky et al.[45, 46] oxygen-oxygen distances between 2.88 and 3.12 Å are obtained for bands appearing between 3490 and 3570 cm^{-1}. These distances are just in the range of O-O distances found by neutron powder diffraction (NPD) for tetragonal[2] or cubic[5] LLZO garnets. On the other hand, the band at 3300 cm^{-1} yields $d_{O\text{-}O}$ = 2.74, which is shorter than the O-O bond distances reported for these garnets. We tentatively propose that short distances arise from the structural rearrangement due to proton insertion into the lattice, although it will be confirmed in a future work from neutron diffraction experiments.

The bands attributed to LiOH and $LiOH{\cdot}H_2O$ disappear upon washing, as expected (inset Fig.2).

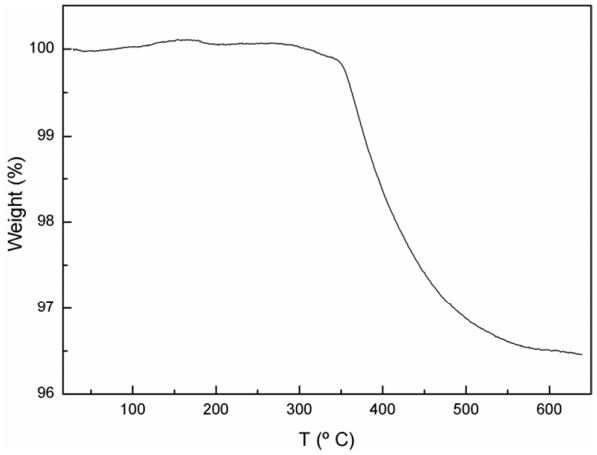

Figure 5. TGA curve of the $^{6}Li_{3.8}H_{3.2}La_3Zr_2O_{12}$ garnet obtained after ageing in air at RT.

In order to gain information about the nature of these protons, ^{1}H-MAS NMR and CP-MAS measurements were carried out in the $Li_{7-x}H_xLa_3Zr_2O_{12}$ system. The ^{1}H-MAS NMR spectra of t-LLZO and $Li_{3.8}H_{3.2}La_3Zr_2O_{12}$ are compared in Fig.6. From the spectrum of t-LLZO it is clear that even the as-prepared tetragonal garnet presents a low proton content, responsible for the weak signal at +4.4 ppm. The band at ~-2ppm is attributed to LiOH formed by proton exchange. After long time exposure to air and washing, the spectrum of $Li_{3.8}H_{3.2}La_3Zr_2O_{12}$ shows a much higher proton content and highlights the presence of at least six other bands (apart from those coming from the rotor) at +10.0, +5.7, +4.4, +3.4, +1.0 and -1.6 ppm, possibly overlapped with other signals of lower intensity. The weak band at negative chemical shifts is attributed to some LiOH formed during sample manipulation,[47] whereas the main bands at +5.7, +4.4, +3.4 and +1.0 ppm are ascribed to protons inside the garnet. These chemical shifts are characteristic of protons involved in weak hydrogen-bonds, and are in agreement with those reported by other authors in analogous cubic compounds exposed to air.[48]

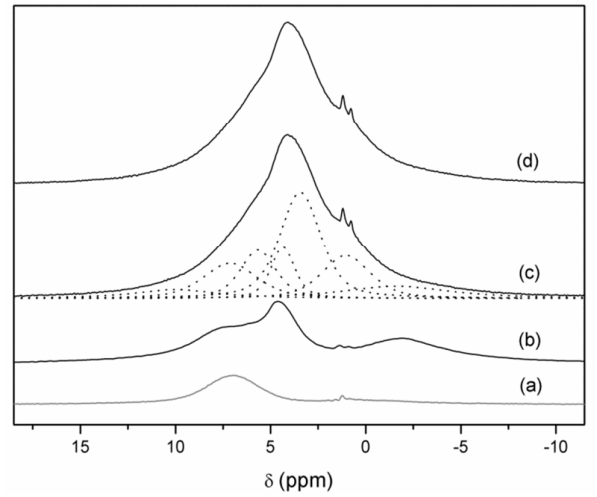

Fig.6. ^{1}H-MAS NMR spectra of $Li_7La_3Zr_2O_{12}$ (b) and $Li_{3.8}H_{3.2}La_3Zr_2O_{12}$ at RT (c) and at 70 °C (d). Dotted lines show the components result of the fitting. The rotor contribution is depicted in (a).

In analogy with the OH^- stretching frequency, different expressions have been proposed to account for the relation between the proton chemical shift and the O-O distance between oxygen atoms involved in the hydrogen-bond. Using for instance the relation given by Eckert et al. [49]:

δ[ppm] = 79.05 - 0.255 $d_{O\text{-}O}$ [pm]

we get d_{O-O}= 2.88, 2.93, 2.97 and 3.06 Å for δ_{iso} = +5.7, + 4.4, + 3.4 and +1.0 ppm, respectively, which are again in the range of O-O distances found for t-LLZO.[2] Both proton NMR and Raman results indicate that protons are quite tightly bound to oxygen anions and that hydrogen bond is weak, which would imply low proton conductivity.

In addition, the presence of a considerable amount of protons in the lattice allows strong cross-polarization effects between protons and lithium ions. Fig.7 (top) shows the ^{6}Li-^{1}H-CP-MAS NMR spectrum of the aged and washed sample. The three bands at +1.6, +1.2 and +0.6 ppm found in single pulse ^{6}Li experiments are still evident, but their relative intensities are very different. A remarkable enhancement of the +0.6 ppm band is observed, which suggests a closer proximity of protons with lithium ions producing that band, previously assigned to tetrahedral coordinated ones. We propose that this behavior may be a consequence of the selective occupancy by protons of the octahedral cavities left vacant by lithium ions upon exchange, in which case the tetrahedral Li sites would be first neighbors for these protons.

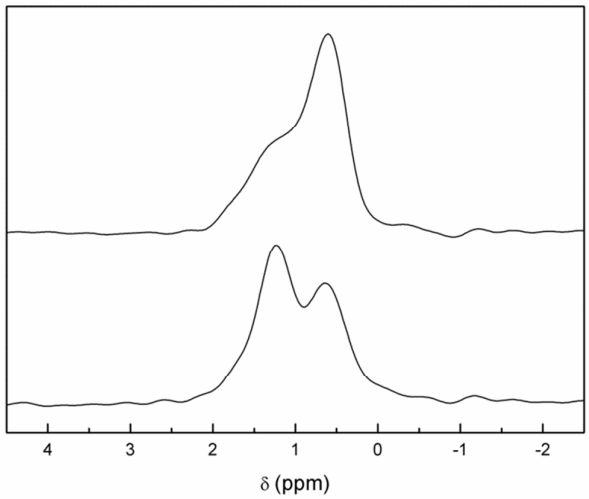

Figure 7. Comparison of ^{6}Li-^{1}H-CP-MAS NMR (top) and ^{6}Li-MAS NMR (with ^{1}H decoupling) (bottom) spectra of $Li_{3.8}H_{3.2}La_3Zr_2O_{12}$

It is interesting to note that preferential occupancy of distorted octahedral cages by protons has been found for proton-exchanged $Li_7Nd_3Zr_2O_{12}$ by modelling techniques.[14] A similar result is found by neutron diffraction for approximately 49% proton-exchanged $Li_5La_3Nb_2O_{12}$.[50] During the revision of this manuscript Li+/H+ exchange of c-LLZO in aqueous solution has been reported[51]. Preferential exchange of the octahedral 96h site is derived from electron energy loss spectroscopy (EELS) experiments in that work.

4. Dynamic effects

Fig.8 shows the temperature evolution of ^{6}Li-MAS and ^{6}Li-^{1}H-CP-MAS NMR spectra of $Li_{3.8}H_{3.2}La_3Zr_2O_{12}$ recorded at RT, 60 °C and 70 °C. The TGA experiment (Fig. 5) shows that there are no significant weight losses at temperatures below 350 °C, which implies that all protons remain in the garnet structure until these temperatures. Both XRD, Raman and ^{1}H-MAS NMR spectra show no changes between RT and 70 °C (see Fig. 6 and Fig. SP2), so ^{6}Li-MAS NMR changes produced at 60 and 70 °C are attributed to a thermally activated motional averaging process in which octahedral and tetrahedral lithium exchange sites. At 70 °C the two components converge to a single symmetric band whose position, +1.1 ppm, agrees within error with the weighted average of the chemical shifts at RT, +1.0 ppm. The fact that the position of the motional-averaged band coincides with the weighted averaged δ_{iso} values means not only that both octahedral and tetrahedral lithium ions are mobile but that they exchange positions, i. e. motion is not restricted to each sublattice separately.

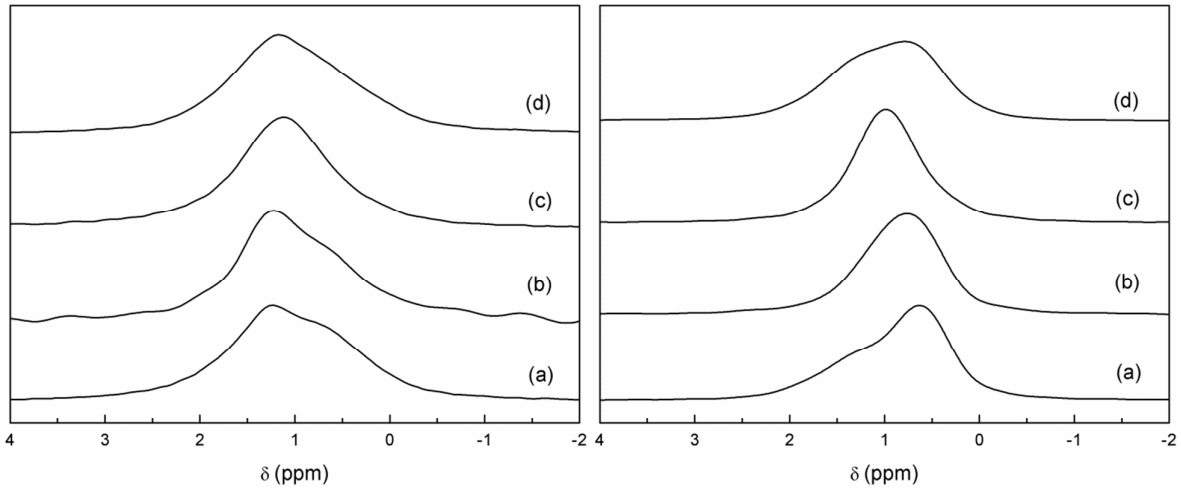

Figure 8. Comparison of ^{6}Li-MAS NMR (left) and ^{6}Li-^{1}H-CP -MAS NMR (right) spectra of $Li_{3.8}H_{3.2}La_3Zr_2O_{12}$ at RT (a), 60 °C (b), 70 °C (c) and at RT after cooling from 70 °C (d).

The remarkable difference between the single pulse MAS and CP MAS-NMR spectra observed at RT, is not found at 70°C, indicating that the preferential transfer of polarization from protons to tetrahedral lithium is affected by the Li dynamic processes. The small discrepancy between the spectra of the sample cooled from 70°C and the pristine sample suggests a slight redistribution of the Li ions in the garnet network.

The occurrence of lithium exchange between tetrahedral and octahedral sites in proton-exchanged LLZO is an interesting phenomenon that deserves further studies. A more detailed variable temperature ^{6}Li-MAS NMR study up to 120 °C of an equivalent sample is compiled in the supplementary information file. As mentioned in section 2, lower T1 values are observed for the two high ppm components corresponding to both octahedral Li sites according to our model. These lower T1 values imply higher mobility, which supports their easier H^+/Li^+ exchange compared to the less mobile tetrahedral Li atoms. It is at higher temperature (between 60 and 90 °C in the present experiments) when these tetrahedral Li atoms attain enough mobility (observable by the decrease in their T1 values) to allow the exchange between sites, yielding an averaging of the position of the NMR bands.

5. Conclusions

The lithium distribution of ^{6}Li-enriched $Li_7La_3Zr_2O_{12}$ has been studied by NMR spectroscopy with XRD and Raman as complementary techniques. The ^{6}Li-MAS-NMR spectrum of as-grown $^{6}Li_7La_3Zr_2O_{12}$ shows a main band at +1.2 ppm and a weak band at ~+0.1 ppm, in agreement with reports of other authors. By combining NMR and Raman spectroscopy the low ppm signal has been definitively identified as coming from Li_2CO_3 and/or $LiOH.H_2O$ resulting from the extreme ability of t-LLZO to undergo Li^+/H^+ exchange when it is exposed to moisture or air, even at RT. When the exchange extent is sufficient and homogeneous, it yields a change in the crystal symmetry from tetragonal to cubic.

The facile Li^+/H^+ exchange has proved to be very useful in the detection and identification of different components beneath the main band at +1.2 ppm, which appear too overlapped to be unambiguously distinguished at first sight. Apart from varying the total lithium content, because of the different stabilities of the tetrahedral and octahedral Li sites, the exchange process also modifies their relative occupation. In the case of the exchanged compound $Li_{3.8}H_{3.2}La_3Zr_2O_{12}$, this change in populations enables the identification of three signals in the ^{6}Li-MAS-NMR spectra, which can be extrapolated to the parent tetragonal compound $Li_7La_3Zr_2O_{12}$. These three signals have been assigned to the three Li environments reported in the literature (from high to low chemical shift: less distorted octahedral, distorted octahedral and tetrahedral). T_1 values obtained from an inversion recovery experiment agree with the different mobilities expected for the different Li sites, the octahedral Li ions being more mobile than the tetrahedral ones. Moreover, measurements at different temperatures have put into evidence the presence of a dynamic process in which octahedral and tetrahedral Li ions exchange sites.

Proton incorporation has been studied by Raman and ^{1}H-MAS-NMR. Both techniques show different signals that can be associated to the presence of non-equivalent oxygen sites in the lattice or to different configurations of proton bonding. The position of these signals in the spectrum suggests the presence of some degree of hydrogen bond.

ACKNOWLEDGMENTS

This work has been supported by the Spanish Ministerio de Economía and Feder funds through grant MAT2010-19837-C06-06 and MAT2010-19837-C06-03. A. Orera and G.Larraz acknowledge the financial support provided by the Spanish *Ministerio de Ciencia e Innovación* through a Juan de la Cierva contract and by Gobierno de Aragón through a PhD grant (B108/11) respectively. The authors wish to thank Servicio General de Apoyo a la Investigacion-SAI (Universidad de Zaragoza) for technical support.

References

1. V. Thangadurai, S. Narayanan and D. Pinzaru, *Chemical Society Reviews*, 2014, **43**, 4714-4727.
2. J. Awaka, N. Kijima, H. Hayakawa and J. Akimoto, *Journal of Solid State Chemistry*, 2009, **182**.
3. J. Percival, E. Kendrick, R. I. Smith and P. R. Slater, *Dalton Transactions*, 2009, 5177-5181.
4. R. Murugan, V. Thangadurai and W. Weppner, *Angewandte Chemie-International Edition*, 2007, **46**, 7778-7781.
5. C. A. Geiger, E. Alekseev, B. Lazic, M. Fisch, T. Armbruster, R. Langner, M. Fechtelkord, N. Kim, T. Pettke and W. Weppner, *Inorganic Chemistry*, 2011, **50**, 1089-1097.
6. M. Kotobuki, K. Kanamura, Y. Sato and T. Yoshida, *Journal of Power Sources*, 2011, **196**.
7. H. Buschmann, J. Doelle, S. Berendts, A. Kuhn, P. Bottke, M. Wilkening, P. Heitjans, A. Senyshyn, H. Ehrenberg, A. Lotnyk, V. Duppel, L. Kienle and J. Janek, *Physical Chemistry Chemical Physics*, 2011, **13**.
8. E. Rangasamy, J. Wolfenstine and J. Sakamoto, *Solid State Ionics*, 2012, **206**.
9. M. A. Howard, O. Clemens, E. Kendrick, K. S. Knight, D. C. Apperley, P. A. Anderson and P. R. Slater, *Dalton Transactions*, 2012, **41**.
10. S. Ohta, T. Kobayashi and T. Asaoka, *Journal of Power Sources*, 2011, **196**.
11. A. Logeat, T. Koehler, U. Eisele, B. Stiaszny, A. Harzer, M. Tovar, A. Senyshyn, H. Ehrenberg and B. Kozinsky, *Solid State Ionics*, 2012, **206**.
12. R. Murugan, S. Ramakumar and N. Janani, *Electrochemistry Communications*, 2011, **13**.
13. R. Takano, K. Tadanaga, A. Hayashi and M. Tatsumisago, *Solid State Ionics*, 2014, **255**, 104-107.
14. M. A. Howard, O. Clemens, K. S. Knight, P. A. Anderson, S. Hafiz, P. M. Panchmatia and P. R. Slater, *Journal of Materials Chemistry A*, 2013, **1**, 14013-14022.
15. K. Meier, T. Laino and A. Curioni, *Journal of Physical Chemistry C*, 2014, **118**, 6668-6679.
16. M. Xu, M. S. Park, J. M. Lee, T. Y. Kim, Y. S. Park and E. Ma, *Physical Review B*, 2012, **85**.
17. R. Jalem, Y. Yamamoto, H. Shiiba, M. Nakayama, H. Munakata, T. Kasuga and K. Kanamura, *Chemistry of Materials*, 2013, **25**, 425-430.
18. R. Bohmer, K. R. Jeffrey and M. Vogel, *Progress in Nuclear Magnetic Resonance Spectroscopy*, 2007, **50**, 87-174.
19. C. P. Grey and N. Dupre, *Chemical Reviews*, 2004, **104**, 4493-4512.
20. J. F. Stebbins, *Solid State Ionics*, 1998, **112**, 137-141.
21. Z. Xu and J. F. Stebbins, *Solid State Nuclear Magnetic Resonance*, 1995, **5**, 103-112.
22. T. M. Alam, S. Conzone, R. K. Brow and T. J. Boyle, *Journal of Non-Crystalline Solids*, 1999, **258**, 140-154.
23. A. Kuhn, M. Kunze, P. Sreeraj, H. D. Wiemhofer, V. Thangadurai, M. Wilkening and P. Heitjans, *Solid State Nuclear Magnetic Resonance*, 2012, **42**, 2-8.
24. C. Galven, J. Dittmer, E. Suard, F. Le Berre and M.-P. Crosnier-Lopez, *Chemistry of Materials*, 2012, **24**, 3335-3345.
25. L. Truong and V. Thangadurai, *Chemistry of Materials*, 2011, **23**, 3970-3977.
26. G. Larraz, A. Orera and M. Sanjuan, *Journal of Materials Chemistry a*, 2013, **1**, 11419-11428.
27. A. Kuhn, S. Narayanan, L. Spencer, G. Goward, V. Thangadurai and M. Wilkening, *Physical Review B*, 2011, **83**.
28. A. Kuhn, J.-Y. Choi, L. Robben, F. Tietz, M. Wilkening and P. Heitjans, *Zeitschrift Fur Physikalische Chemie-International Journal of Research in Physical Chemistry & Chemical Physics*, 2012, **226**.
29. L. van Wullen, T. Echelmeyer, H. W. Meyer and D. Wilmer, *Physical Chemistry Chemical Physics*, 2007, **9**, 3298-3303.
30. M. Nyman, T. M. Alam, S. K. McIntyre, G. C. Bleier and D. Ingersoll, *Chemistry of Materials*, 2010, **22**, 5401-5410.

31. T. L. Spencer, N. W. Plagos, D. H. Brouwer and G. R. Goward, *Physical Chemistry Chemical Physics*, 2014, **16**, 2515-2526.
32. S. Ramakumar, L. Satyanarayana, S. V. Manorama and R. Murugan, *Physical Chemistry Chemical Physics*, 2013, **15**, 11327-11338.
33. S. Narayanan, F. Ramezanipour and V. Thangadurai, *Journal of Physical Chemistry C*, 2012, **116**.
34. A. Gupta, R. Murugan, M. P. Paranthaman, Z. Bi, C. A. Bridges, M. Nakanishi, A. P. Sokolov, K. S. Han, E. W. Hagaman, H. Xie, C. B. Mullins and J. B. Goodenough, *Journal of Power Sources*, 2012, **209**.
35. M. P. O'Callaghan, A. S. Powell, J. J. Titman, G. Z. Chen and E. J. Cussen, *Chemistry of Materials*, 2008, **20**, 2360-2369.
36. B. Koch and M. Vogel, *Solid State Nuclear Magnetic Resonance*, 2008, **34**, 37-43.
37. A. Kuhn, V. Epp, G. Schmidt, S. Narayanan, V. Thangadurai and M. Wilkening, *Journal of physics. Condensed matter : an Institute of Physics journal*, 2012, **24**.
38. S. Narayanan, V. Epp, M. Wilkening and V. Thangadurai, *Rsc Advances*, 2012, **2**.
39. H. M. Rietveld, *Journal of Applied Crystallography*, 1969, **2**, 65-&.
40. J. Rodriguezcarvajal, *Physica B*, 1993, **192**, 55-69.
41. E. J. Cussen, *Journal of Materials Chemistry*, 2010, **20**, 5167-5173.
42. C. Galven, E. Suard, D. Mounier, M.-P. Crosnier-Lopez and F. Le Berre, *Journal of Materials Research*, 2013, **28**, 2147-2153.
43. D. Wang, G. Zhong, O. Dolotko, Y. Li, M. J. McDonald, J. Mi, R. Fu and Y. Yang, *Journal of Materials Chemistry A*, 2014.
44. K. Beckenkamp and H. D. Lutz, *Journal of Molecular Structure*, 1992, **270**, 393-405.
45. E. Libowitzky, *Monatshefte Fur Chemie*, 1999, **130**, 1047-1059.
46. T. Steiner, *Angewandte Chemie (International ed. in English)*, 2002, **41**, 49-76.
47. Y. Y. Hu, Z. G. Liu, K. W. Nam, O. J. Borkiewicz, J. Cheng, X. Hua, M. T. Dunstan, X. Q. Yu, K. M. Wiaderek, L. S. Du, K. W. Chapman, P. J. Chupas, X. Q. Yang and C. P. Grey, *Nature Materials*, 2013, **12**, 1130-1136.
48. C. Bernuy-Lopez, W. Manalastas, J. M. Lopez del Amo, A. Aguadero and J. A. Kilner, Chemistry of Materials, 2014, pp. 3610-3617.
49. H. Eckert, J. P. Yesinowski, L. A. Silver and E. M. Stolper, *Journal of Physical Chemistry*, 1988, **92**, 2055-2064.
50. L. Truong, M. Howard, O. Clemens, K. S. Knight, P. R. Slater and V. Thangadurai, *Journal of Materials Chemistry A*, 2013, **1**, 13469-13475.
51. C. Ma, E. Rangasamy, C. Liang, J. Sakamoto, K. L. More and M. Chi, *Angewandte Chemie International Edition*, 2015, **54**, 129-133.

Graphical Abstract

We present a NMR study of enriched $^{6}Li_{7-x}H_xLa_3Zr_2O_{12}$ ($0 \leq x \leq 5$) garnets for the study of the distribution of the lithium ions in $Li_7La_3Zr_2O_{12}$ and their contribution to ionic conductivity. Taking advantage of the facile proton-for-lithium exchange, we have been able to alter the relative population of tetrahedral and octahedral sites by submitting the samples to different post-treatments so as to obtain samples with varying lithium content. This has allowed the identification of three different bands that we ascribe to Li in different environments within the garnet structure. Besides, variable temperature measurements have put into evidence the presence of dynamic processes between octahedral and tetrahedral Li sites. Protons inserted in the garnet structure have also been analyzed by means of ^{1}H-MAS-NMR, ^{6}Li-^{1}H-CP-MAS-NMR and Raman spectroscopies.